The Road to Personalized Myeloma Medicine: Patient-specific Single-domain Antibodies for Anti-idiotypic Radionuclide Therapy

Janik Puttemans[1], Benoit Stijlemans[2,3], Marleen Keyaerts[1,4], Sam Vander Meeren[5], Wim Renmans[5], Karel Fostier[6,7], Pieterjan Debie[1], Heleen Hanssens[1], Magdalena Rodak[8], Marek Pruszynski[8,9], Kim De Veirman[10], Karin Vanderkerken[10], Tony Lahoutte[1,4], Alfred Morgenstern[11], Frank Bruchertseifer[11], Nick Devoogdt[1], and Matthias D'Huyvetter[1]

ABSTRACT

To this day, multiple myeloma remains an incurable cancer. For many patients, recurrence is unavoidably a result of lacking treatment options in the minimal residual disease stage. This is due to residual and treatment-resistant myeloma cells that can cause disease relapse. However, patient-specific membrane-expressed paraproteins could hold the key to target these residual cells responsible for disease recurrence. Here, we describe the therapeutic potential of radiolabeled, anti-idiotypic camelid single-domain antibody fragments (sdAbs) as tumor-restrictive vehicles against a membrane-bound paraprotein in the syngeneic mouse 5T33 myeloma model and analogously assess the feasibility of sdAb-based personalized medicine for patients with multiple myeloma. Llamas were immunized using extracts containing paraprotein from either murine or human sera, and selective sdAbs were retrieved using competitive phage display selections of immune libraries. An anti-5T33 idiotype sdAb was selected for targeted radionuclide therapy with the β^--particle emitter ^{177}Lu and the α-particle emitter ^{225}Ac. sdAb-based radionuclide therapy in syngeneic mice with a low 5T33 myeloma lesion load significantly delayed tumor progression. In five of seven patients with newly diagnosed myeloma, membrane expression of the paraprotein was confirmed. Starting from serum-isolated paraprotein, for two of three selected patients anti-idiotype sdAbs were successfully generated.

Introduction

Multiple myeloma is the second most common hematologic cancer, accounting for 15% of blood cancers and 2% of all cancers (1). It originates in the bone marrow (BM) with an uncontrolled proliferation of terminally differentiated plasma cells. Under normal circumstances, plasma cells produce a wide variety of immunoglobulins (Ig) to fight off infections. With the clonal expansion of malignant plasma cells comes severe B-cell suppression and the excessive secretion of a certain patient-specific mAb or antibody fragment, termed the M-protein or paraprotein. Malignant plasma cells nested in the BM are associated with lytic bone lesions due to increased osteoclast and decreased osteoblast activity, causing calcium to leak into the extracellular fluid. Because of the end-organ destruction, mainly related to BM and kidneys, multiple myeloma is associated with a high lethality. Despite improvements made in chemotherapeutic treatment options and the availability of therapies targeting the myeloma cells and/or the microenvironment, patients still experience almost universal recurrence (2, 3). In addition, not all patients are eligible for high-dose chemotherapy and autologous stem cell transplantation due to old age, limiting their therapeutic options. Because of the unavoidable relapse, multiple myeloma is still considered as an incurable disease for most patients (4). Therapy-resistant myeloma cells can nest in the bone marrow and remain dormant for years. This subset of progenitor cells can later mediate tumor regrowth, even after high-dose melphalan therapy. Importantly, these progenitor cells may not express common multiple myeloma biomarkers, such as CD38 or CD138, which could proof to be a bottleneck for the development of targeted therapies (5).

It has been reported that in 35% of diagnosed multiple myeloma cases, the paraprotein—which is normally secreted in high amounts—is also anchored to the surface of malignant plasma cells (6–8). This phenomenon has been confirmed using single-cell transcriptome analysis of dormant murine myeloma cells (9). The expressed paraprotein's sequence is unique for each patient's multiple myeloma. It is defined by unique complementarity-determining regions, which are referred to as the "idiotype" (Id). This makes surface expression of the patient's paraprotein a valuable tumor-specific antigen to develop targeted therapies to overcome acquired treatment resistance. Highly specific, anti-Id compounds might therefore be promising tumor- and patient-specific vehicles for tumor therapy. To this end, single-domain antibody fragments (sdAbs) have been shown to possess favorable characteristics in terms of fast tumor targeting and clearance from

[1]Department of Medical Imaging, Laboratory for In Vivo Cellular and Molecular Imaging, Vrije Universiteit Brussel, Brussels, Belgium. [2]Department of Cellular and Molecular Immunology, Vrije Universiteit Brussel, Brussels, Belgium. [3]Myeloid Cell Immunology Lab, VIB Center for Inflammation Research, Brussels, Belgium. [4]Nuclear Medicine Department, UZ Brussel, Brussels, Belgium. [5]Department of Clinical Biology, Hematology Division, UZ Brussel, Brussels, Belgium. [6]Department of Hematology, OLV Aalst, Aalst, Belgium. [7]Department of Hematology, UZ Brussel, Brussels, Belgium. [8]Institute of Nuclear Chemistry and Technology, Warsaw, Poland. [9]Faculty of Chemistry, University of Warsaw, Warsaw, Poland. [10]Department of Hematology and Immunology, Vrije Universiteit Brussel, Brussels, Belgium. [11]European Commission, Joint Research Centre, Directorate for Nuclear Safety and Security, Karlsruhe, Germany.

Note: Supplementary data for this article are available at Molecular Cancer Therapeutics Online (http://mct.aacrjournals.org/).

N. Devoogdt and M. D'Huyvetter contributed equally to this article.

Corresponding Author: Matthias D'Huyvetter, Department of Medical Imaging, Vrije Universiteit Brussel, Laarbeeklaan 103, Building K, Brussels 1090, Belgium. Phone: 322-477-4991; E-mail: matthias.dhuyvetter@vub.be

Mol Cancer Ther 2022;21:159–69

doi: 10.1158/1535-7163.MCT-21-0220

nontarget tissues (10). sdAbs are the antigen-binding fragments that are derived from *camelidae* heavy-chain-only antibodies. They are about 10 times smaller than conventional antibodies, not immunogenic, have nanomolar affinities and are produced in high yields with high stability. Their small size leads to better tissue penetration, favorable pharmacologic properties, and together with a longer antigen recognizing region they are capable of recognizing small, buried epitopes (11, 12).

For preclinical validation, the 5TMM murine models provide syngeneic, transplantable, immunocompetent models that resemble human multiple myeloma clinically and biologically. The most studied are the 5T2MM and the more aggressive, fast-growing 5T33MM models (13, 14). Earlier, we described the generation and characterization of the anti-5T2MM idiotype (5T2MMid) sdAb R3B23 and demonstrated its therapeutic potential for targeted radionuclide therapy (TRNT) (15). Despite the proven value of sdAb-based anti-Id TRNT, the anti-5T2MMid sdAb R3B23 was generated using highly purified 5T2MM paraprotein. The feasibility of this approach, however, has not been demonstrated for clinical translation, where only crude serum-Ig purification is available. Here we describe the generation of a novel anti-5T33MMid sdAb, based on serum-Ig-immunization of the same quality as clinically available samples. This anti-5T33MMid sdAb was radiolabeled with the β^--particle emitter ^{177}Lu (half-life: 6.7 days) and the α-particle emitter ^{225}Ac (half-life: 10 days), and evaluated for therapeutic efficacy in tumor-bearing mice in a setting artificially mimicking minimal residual disease (MRD) of multiple myeloma. The presence of membrane-anchored idiotype was evaluated in patients with newly diagnosed myeloma. Patient-specific anti-idiotypic sdAb generation and screening was performed analogously after crude serum-Ig purification for three patients.

Materials and Methods

All reagents used in cell culture experiments were purchased from Gibco BRL except when noted. All other reagents were purchased from Sigma-Aldrich except when noted. Anti-5T2MMid sdAb R3B23, used as a control sdAb, was generated as described previously (15).

Cell culture conditions

The 5T33MMvivo cells originate spontaneously in ageing C57BL/KaLwRij mice. The 5T33MMvitro is a clonally identical variant that originated spontaneously from an *in vitro* culture of 5T33MMvivo cells and were generously provided by Jiri Radl. This myeloma cell line grows *in vitro* in a stroma-independent manner and cells were cultured in RPMI1640 growth medium enriched with 10% FBS, 1% L-glutamine, 1% nonessential amino acids, 100 U/mL penicillin, and 0.01% streptomycin (Invitrogen). Cells were grown in a humidified atmosphere with 5% CO_2 at 37°C. Absence of *Mycoplasma* was confirmed (Venor GeM Mycoplasma Detection Kit) before the start of *in vitro* experiments. Cells were used within five to 10 passages after generation or thawing.

Animal models

All animal experiments were approved by the Institutional Animal Care and Use Committee (Ethical Committee for Animal Experiments) of the Vrije Universiteit Brussel (license No. LA1230281/1230272, dossier 17-272-8). 5T33MMvivo cells were isolated from 10 weeks old, diseased C57BL/KalwRij mice (Envigo) by flushing the BM out of the femurs and tibiae and crushing the vertebrae to release BM cells. BM mononuclear cells were purified by Lympholyte M (Cedarlane) gradient centrifugation at 1,000 rcf for 20 minutes. These cells were used for intravenous (i.v.) injection into young syngeneic mice.

Monoclonal Id (5T33MMid) and anti-Id mAb 3H2 were produced and purified as described previously (13). For experimental purposes, 6-week-old female C57BL/KalwRij mice were intravenously injected with 5×10^5 5T33MMvivo cells. For biodistribution and dosimetry studies, 6-week-old female C57BL/6 mice (Charles River) were used.

Anti-5T33MMid sdAb generation and screening

Two murine antigen preparations were prepared out of sera from C57BL/KalwRij mice containing the 5T33MMid paraprotein. The IgG fraction was purified from these sera using a Protein G Sepharose 4 Fast Flow column and will be referred to as 5T33-protein G antigen. This preparation contains IgGs from the complete immune repertoire but is highly dominated by the 5T33MMid. This IgG fraction was also further purified on a CNBr-Activated Sepharose 4 Fast Flow affinity column (Cytiva) conjugated with the anti-Id mAb 3H2 specific for the 5T33MMid and will be referred to as the 5T33-pure antigen. sdAb generation was performed by the Nanobody Service Facility [Vlaams Instituut voor Biotechnologie (VIB, Brussels, Belgium)] as described before (16). Briefly, a llama was subcutaneously injected on days 0, 7, 14, 21, 28, and 35, each time with about 100 μg of 5T33-protein G antigen with GERBU adjuvant LQ 3000 (GERBU Biotechnik; Ethical dossier Lamasté 2020–1). On day 40, anticoagulated blood was collected for the preparation of peripheral blood lymphocytes (PBLs). Total RNA from PBLs was used as a template for cDNA synthesis. The variable domains of the heavy-chain-only antibodies (i.e., sdAbs) were amplified in a two-step PCR, digested with *PstI* and *NotI*, and cloned into the phagemid vector pMECS. The ligated material was transformed into electrocompetent *E. coli* TG1 cells, hereby generating an immune sdAb library of approximately 10^9 independent transformants.

The phage-displayed library was first panned on solid phase–coated 5T33-pure antigen for three rounds to gauge the extent of the response to the 5T33MMid antibodies. The binding of phages to 5T33-pure antigen coated on the well was competed by the inclusion of a mix of mouse $IgG_{2b}\kappa$ (5T33MMid isotype) and mouse total IgG, each at a final concentration of 1 μmol/L, during biopanning. In total, 190 colonies were randomly selected and analyzed by ELISA for the presence of antigen-specific sdAbs in their periplasmic extracts. The antigen used for the ELISA screening was the same 5T33-pure antigen as the one used for panning, using three negative controls as follows: wells coated with either mouse $IgG_{2b}\kappa$ or total mouse IgG, and uncoated blocked wells.

Next, the library was panned on the 5T33-protein G antigen to gauge the amount of sdAbs overlapping with the 5T33-pure set. The panning was performed as described previously except that the binding of phages to 5T33-protein G antigen coated on the well was competed only by 1 μmol/L mouse total IgG. In total, 190 colonies were randomly selected and analyzed by ELISA for the presence of antigen-specific sdAbs in their periplasmic extracts. Both the 5T33-protein G and the 5T33-pure antigen were separately used for the ELISA screening. As above, wells coated with either mouse $IgG_{2b}\kappa$ or total mouse IgG, and uncoated blocked wells were used as negative controls. Periplasmatic extracts containing the hemagglutinin (HA)-His_6-tagged sdAbs were obtained by applying a freeze-thawing cycle to pelleted cells of 1-mL bacterial culture cells after adding isopropyl-β-d-thiogalactoside, as described before (16). Bound

sdAbs were detected via a primary mouse IgG_1 anti-HA antibody (Sigma-Aldrich, catalog No. SAB2702217, RRID:AB_2750919) and secondary rat anti-mouse IgG_1 antibody, coupled to alkaline phosphatase (Abcam, catalog No. ab99602, RRID:AB_10674628), which after addition of 4-nitrophenyl phosphate causes a color shift that can be measured at 405 nm (VERSA max microplate reader, Molecular Devices). After nucleotide sequencing, based on similarities in their protein sequence, positive scoring clones are divided into different CDR3 groups.

Off-rate screening and affinity determination of anti-5T33MMid sdAbs by surface plasmon resonance

Surface plasmon resonance (SPR) measurements were performed on a Biacore T200 instrument (GE Healthcare). 5T33-pure antigen was coupled on a CM5 chip to 2000 response units. All analytes were flown at 30 μL/minute in Hanks' Balanced Salt Solution (HBSS), and the chip was regenerated using glycine-HCl (10 mmol/L, pH 1.5). For off-rate screening, sensorgrams of the dissociation phase were generated of periplasmic extracts, filtered and diluted 1/2 in HBSS. For determination of binding kinetics, sensorgrams were generated of serial 1/2-diluted purified sdAb solutions. Binding was allowed for 180 seconds and dissociation for 600 seconds. Curves were fitted using Biacore's evaluation software using a 1:1 antigen:analyte binding model with drift and RI2 correction to retrieve association rate constants (k_{on}), dissociation rate constants (k_{off}), and equilibrium dissociation constants (K_D, a measurement of affinity).

sdAb binding on cell-expressed 5T33MMid paraprotein via flow cytometry

5T33MMvitro cells were collected, washed, and counted. Per 5×10^5 cells, either 100-μL periplasmic extract, 1-μg purified His_6-tagged sdAb or 1-μg anti-5T33MMid antibody 3H2 was added and incubated for 1 hour at 4°C. sdAb binding was detected by sequential 1-hour incubations at 4°C with 1-μg anti-HA mouse IgG_1 or anti-His mouse IgG_1 antibody and 200-ng PE-coupled anti-mouse IgG_1 antibody (BD Biosciences). 3H2 binding was detected by 1-hour incubations at 4°C with 200-ng PE-coupled anti-mouse IgG_1 antibody (BD Biosciences). Wells were washed three times with PBS-1% BSA between each step. Samples were measured using a BD FACSCelesta flow cytometer (BD Biosciences).

Evaluation of ^{99m}Tc-labeled sdAb biodistribution via μSPECT/CT imaging and *ex vivo* dissection analyses

For each sdAb-candidate, naïve C57BL/KaLwRij ($n = 3$) and late-stage 5T33MM-diseased mice ($n = 3$, 21 days postinoculation of 5T33vivo cells) were intravenously injected with 105 ± 12 MBq (5-μg protein) ^{99m}Tc-labeled sdAb. ^{99m}Tc radiolabeling was performed as described in Supplementary Materials and Methods. [^{99m}Tc]Tc-$(CO)_3$-His_6-sdAbs will be referred to as [^{99m}Tc]-sdAbs.

At 1-hour postinjection mice were imaged using pinhole μSPECT/CT with a Vector+/CT MILabs system under 2.5% isoflurane anesthesia. SPECT images were obtained using a rat SPECT collimator (1.5-mm pinholes) in spiral mode, nine positions with 50 seconds per position for whole-body imaging, resulting in an 8-minute SPECT scan time. Images were reconstructed with 0.4 mm^3 voxels with two subsets and two iterations, without a postreconstruction filter. For CT, a normal scan mode of only one position of 2 minutes was used. Images were fused and corrected for attenuation based on the CT scan. Image analysis was performed using a Medical Image Data Examiner (AMIDE) software (17). After imaging, mice were sacrificed at 70 minutes postinjection, and organs and tissues were isolated and weighed. The radioactivity in each sample was measured using a Wizard2 γ-counter (PerkinElmer). Tracer uptake was expressed as % injected activity per gram organ (%IA/g).

Idiotype-targeted radionuclide therapy during MRD stage

Conjugation to bifunctional chelators and radiolabeling is described in Supplementary Materials and Methods. Naïve 6-week-old female C57BL/KaLwRij mice were intravenously injected with 5×10^5 5T33MMvivo cells/mouse. Starting at day 4 after tumor inoculation, when serum paraprotein was still undetectable, mice were divided into three treatment groups ($n = 16$/group). Treatments were administered on days 4, 7, 10, and 13 after tumor inoculation. Mice were euthanized when weight loss exceeded 20%, or at the advent of paralysis of the hind limbs.

In the first treatment experiment, one treatment group received four i.v. saline buffer injections, one treatment group received four i.v. injections of 10.4 ± 1.1 MBq [^{177}Lu]Lu-DTPA-R3B23 control sdAb, and one treatment group was administered four i.v. injections of 10.5 ± 0.7 MBq [^{177}Lu]Lu-DTPA-8379 anti-5T33MMid sdAb. [^{177}Lu]Lu-DTPA-sdAb will be referred to as [^{177}Lu]-sdAb. When seven mice of the saline buffer group reached humane endpoint criteria for euthanasia, three mice from each treatment group were sacrificed for analysis and were excluded from the survival experiment outcome. Radioactive tracer uptake in the bone was measured using a Wizard2 γ-counter (PerkinElmer) and spleens were isolated and weighed.

In a second treatment experiment, one treatment group received four intravenous saline buffer injections, one treatment group received four intravenous injections of 50.2 ± 2.4 kBq [^{225}Ac]Ac-DOTA-R3B23 control sdAb, and one treatment group was administered four intravenous injections of 48.9 ± 1.5 kBq [^{225}Ac]Ac-DOTA-8379 anti-5T33MMid sdAb. When seven mice of the saline buffer group reached humane endpoint criteria for euthanasia, three mice from each treatment group were sacrificed for analysis and were excluded from the survival experiment outcome. Radioactive tracer uptake in the bone was measured using a Wizard2 γ-counter (PerkinElmer) and spleens were isolated and weighed.

^{177}Lu- and ^{225}Ac-labeled sdAbs were coadministered with 150 mg/-kg of the plasma expander Gelofusine (B. Braun; ref. 18). [^{225}Ac]Ac-DOTA-sdAb will be referred to as [^{225}Ac]-sdAb.

Patient-specific anti-idiotypic sdAb generation and screening

Patients with newly confirmed multiple myeloma were enrolled for a single-center, prospective clinical trial (NCT03956615). This study was approved by the Universitair Ziekenhuis Brussel Ethical Committee and was performed in accordance with the Council for International Organizations of Medical Sciences (CIOMS) ethical guidelines. All participants had given written informed consent prior to the investigation. Inclusion criteria were (i) patients were at least 18 years old; (ii) patients were scheduled to undergo BM sampling in clinical routine because of a clinically suspected or pathologically confirmed multiple myeloma.

Patients underwent BM sampling and plasma cells were analyzed for membrane expression of paraprotein via flow cytometry (Cytomics FC500 Flow Cytometer, Beckman Coulter). Malignant plasma cells were selected on the basis of high CD38 expression (anti–CD38-PE, clone HB-7, BD Biosciences). Patients with confirmed membrane-anchored, paraprotein-expressing plasma cells were subjected to a blood sampling of 10 mL by venous puncture, after which the paraprotein-containing serum was purified using a protein G column. The purified fraction will be referred to as "idiotype-protein G." sdAb generation was performed by the Nanobody Service Facility (VIB,

Brussels, Belgium) as described previously. The library was panned on solid phase–coated idiotype-protein G (100 μg/mL in 100 mmol/L $NaHCO_3$, pH 8.2) for three rounds. To avoid enrichment of non-anti-Id sdAbs, the binding of phages to the conserved regions of the used human Ig isotype was competed with a mixture of total human Ig isotype (same isotype as patient-specific paraprotein) in solution, each at a final concentration of 1 μmol/L. Colonies were randomly selected from panning rounds two and three, and analyzed by ELISA for the presence of anti-Id sdAbs in their periplasmic extracts. As was mentioned, wells coated with total human Ig isotype (same isotype as patient-specific paraprotein) and uncoated blocked wells were used as negative controls. The antigen used for panning and ELISA screening was the same as the one used for immunization.

Statistical analysis

For statistical analysis and survival analysis, the unpaired two-tailed *t* test and log-rank (Mantel–Cox) tests were performed. $P < 0.05$ was considered as statistically significant, with *, $P < 0.05$; **, $P < 0.01$; and ***, $P < 0.001$. Results are given as mean ± SD.

Results

Immunization of a llama with serum 5T33-protein G and competitive biopannings resulted in highly 5T33MMid-specific sdAbs

A llama was immunized with the IgG fraction containing 5T33MMid paraprotein from sera of late-stage diseased mice (i.e., 5T33-protein G antigen), following standard protocols. Panning was performed using either 5T33-protein G antigen, or an anti–Id-purified 5T33MMid paraprotein (i.e., 5T33-pure antigen), in the presence of aspecific IgG to enrich for anti-Id sdAbs. Out of both panning strategies, 190 potential sdAb candidates were screened via ELISA on 5T33-pure antigen, isotype control IgG and aspecific total mouse IgG. Samples were considered as 5T33 anti-idiotypic when the measured absorbance on 5T33-pure antigen was three times higher than the other signals. Of the 190 5T33-protein G antigen-panned colonies, 135 colonies were anti-idiotypic. On the basis of sequence data of the positive clones, 102 different sdAbs were distinguished, belonging to 37 different CDR3 groups.

Of the 190 5T33-pure antigen-panned colonies, 147 colonies scored positive in this assay. On the basis of sequence data of the positive clones, 85 different sdAbs were distinguished. Taking the overlap with 5T33-protein G antigen-panned clones into account, 72 unique anti-5T33 idiotype sdAbs were found belonging to 34 different CDR3.

The 5T33-protein G antigen panning had 37 CDR3 groups, of which 15 were shared with the 5T33-pure antigen panning, leaving 22 (mostly single clone) CDR3 groups unique to IgG panning. Similarly, the 5T33MMid panning had 19 groups unique to this panning.

High-throughput screening of 5T33MMid-specific sdAbs resulted in lead candidates from both panning methods

All unique anti-5T33MMid sdAbs were subjected to off-rate screening via SPR on immobilized 5T33-pure antigen (**Fig. 1A**), as well as via flow cytometry for their ability to bind cell-bound 5T33MMid (**Fig. 1B**). These first two screening methods were performed on unpurified periplasmic extracts from small-scale 1-mL bacterial cultures. From these tests, 10 sdAb candidates were selected with cellular binding and the lowest k_{off} value. An overview of the best scoring sdAbs is represented in **Table 1**, along with the mean fluorescent intensity values from flow cytometry and whether the sdAb was obtained from the 5T33-protein G or 5T33-pure panning.

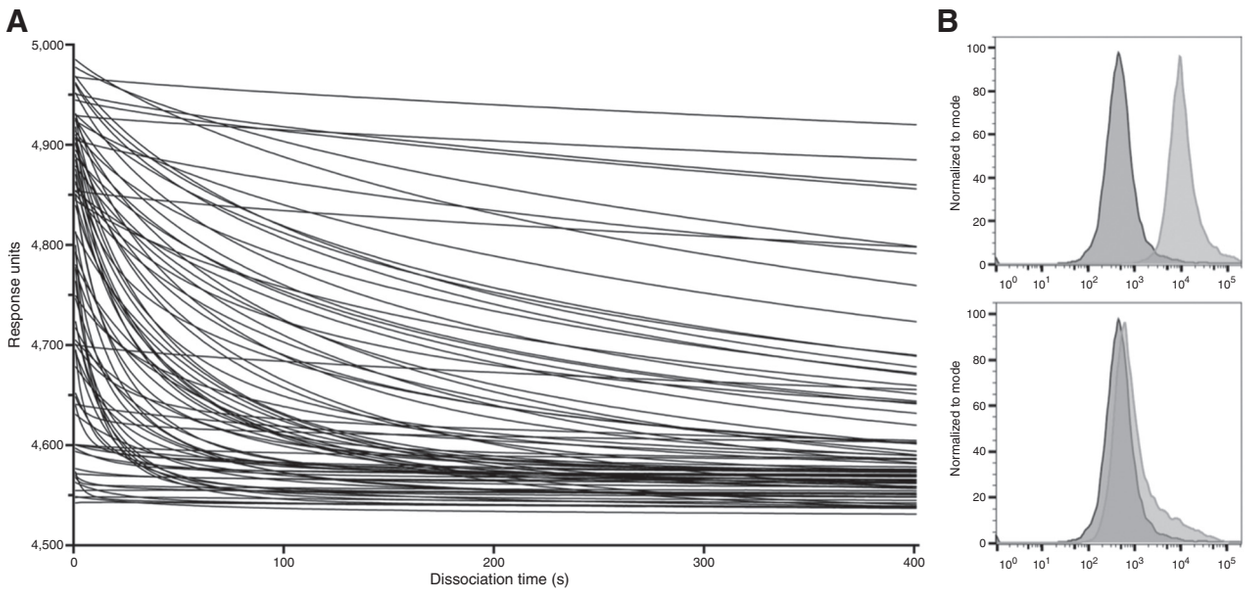

Figure 1.

Primary screening of sdAb library. **A,** SPR sensorgrams of the dissociation phase of sdAb-containing periplasmic extracts. Sensorgrams with a slowly descending response unit (RU) slope generally signify a higher affinity toward their target, whereas sensorgrams that show a fast decrease in RU are quickly dissociated from their target, resulting in a low affinity. **B,** Representative graphs of specific cell-expressed 5T33MMid recognition by sdAb candidates, measured via flow cytometry. A 5T33MMid-binding sdAb candidate (8379) causes a shift in mean fluorescent intensity (top, light gray), whereas anti-5T2MMid control sdAb R3B23 shows minimal background signal on 5T33MMvitro cells (bottom, light gray). Shift in mean fluorescent intensity is measured against isotype control staining (dark gray).

Table 1. Overview of first selection of sdAb candidates.

	ELISA	SPR	Flow cytometry	Panning method	
sdAb	$Abs_{5T33MMid}/Abs_{IgG2b\kappa}$	k_{Off} (s^{-1})	ΔMFI	5T33-Protein G	5T33-pure
8379	33.95	1.45E-03	6181	Yes	Yes
8311	32.27	1.54E-03	5262	Yes	Yes
8326	28.65	1.98E-03	5353	Yes	Yes
8351	32.88	2.70E-03	4925	Yes	Yes
8387	32.29	2.55E-03	4434	No	Yes
8404	30.43	2.25E-03	7716	No	Yes
8335	32.78	2.25E-03	4287	No	Yes
8928	38.52	1.87E-03	5271	Yes	No
8954	32.34	2.03E-03	4971	Yes	No
8946	33.10	2.23E-03	3582	Yes	No

Note: Each sdAb is represented with its respective 5T33MMid/$IgG_{2b}\kappa$ absorbance (Abs) ratio obtained via ELISA, dissociation constant (k_{Off}) value obtained via SPR, mean fluorescent intensity (ΔMFI) via flow cytometry, and whether it was discovered in the 5T33-protein G and/or 5T33-pure panning method.

Lead selection of purified anti-5T33MMid sdAbs

The most promising sdAbs from the initial screening rounds (sequences in Supplementary Table S1; Genbank accession numbers OK268233-OK268241) were recloned into a pHEN6-production vector and purified. First, SPR analysis of His_6-tagged sdAbs on immobilized 5T33MMid paraprotein was performed to determine binding kinetics parameters (**Table 2**). Almost all sdAbs bound to the paraprotein with affinities in the low nanomolar range. sdAb 8311 had a K_D value of 380 pmol/L, making it the highest affinity candidate. SdAb 8946 had the worst affinity of 77.4 nmol/L and was excluded from further testing. A representative sensorgram of sdAb 8379 is given in Supplementary Fig. S1A.

Second, sdAbs were radiolabeled with ^{99m}Tc for further *in vitro* and *in vivo* evaluation. Radiolabeling of all sdAbs with ^{99m}Tc resulted in a radiochemical purity >95%, apart from sdAb 8335, which did not reach a purity above 50% and was excluded from further screening assays. Radioligand cell-binding saturation studies of all ^{99m}Tc-labeled sdAbs on 5T33MMvitro cells revealed binding kinetics varying from low to high nanomolar affinities (**Table 2**). [^{99m}Tc]-8954 and [^{99m}Tc]-8928 had significantly lower affinity values in the radioligand binding assay and were excluded for further testing. A representative saturation curve of [^{99m}Tc]-8379 is given in Supplementary Fig. S1B.

On the basis of these results, six sdAb candidates were selected for *in vivo* biodistribution screening. sdAbs were radiolabeled with ^{99m}Tc and were intravenously injected in both healthy and late-stage 5T33MM-bearing mice with high levels of circulating paraprotein. Radiochemical purity was above 95% after purification. One hour postinjection, mice (n = 3/group) were subjected to a full-body μSPECT/CT scan, killed, and their organs were collected for *ex vivo* radioactive uptake quantification. As illustrated in **Fig. 2A** and **B**, [^{99m}Tc]-sdAbs showed a high kidney and bladder uptake in healthy mice, whereas tumor-bearing mice also show uptake in highly vascularized organs, such as liver and heart. These findings were confirmed in the *ex vivo* analysis of organs and tissues (**Fig. 2C** and **D**). All sdAbs showed favorable distribution through the body of healthy mice with fast clearance through the kidneys and bladder, except for [^{99m}Tc]-8311, which showed high uptake in bone, liver, heart, lungs, and the stomach. [^{99m}Tc]-8404 showed remarkably high kidney uptake. In late-stage 5T33MM-bearing mice, all sdAb candidates show high activities in blood and highly vascularized organs such as heart, liver, lungs, and the spleen due to interaction with circulating paraprotein (**Fig. 2B**). [^{99m}Tc]-8379 showed the highest ratio of blood $activity_{diseased}$/blood $activity_{healthy}$ of 92.4 ± 45.4, whereas [^{99m}Tc]-8404 had the lowest ratio of 6.8 ± 1.8. ^{99m}Tc-labeled sdAb R3B23, which was previously shown to be anti-idiotypic for another, 5T2MM paraprotein (15) showed low accumulation within the body or blood, apart from kidneys and bladder. The blood $activity_{diseased}$/blood $activity_{healthy}$ ratio for [^{99m}Tc]-R3B23 was

Table 2. Determination of equilibrium dissociation constant K_D and EC_{50} of purified sdAbs.

	SPR			Radioligand binding assay
sdAb	k_{on} ($M^{-1}s^{-1}$)	k_{off} (s^{-1})	K_D (nmol/L)	EC_{50} (nmol/L)
8379	2.83×10^5	5.48×10^{-4}	1.94	3.15
8311	6.27×10^5	2.39×10^{-4}	0.38	0.94
8326	9.84×10^5	10.6×10^{-4}	1.08	14.57
8351	4.66×10^5	5.93×10^{-4}	1.27	19.54
8387	3.18×10^5	12.8×10^{-4}	4.03	8.54
8404	2.67×10^5	14.6×10^{-4}	5.47	32.0
8335	10.6×10^5	23.1×10^{-4}	2.18	ND
8928	10.5×10^5	23.1×10^{-4}	2.18	67.5
8954	1.46×10^5	19.9×10^{-4}	13.6	52.0
8946	1.73×10^5	134×10^{-4}	77.4	ND

Note: K_D values were calculated on the basis of association (k_{on}) and dissociation constants (k_{off}) via SPR on immobilized 5T33MMid paraprotein, as well as via saturation binding assay of radiolabeled sdAbs on 5T33MMvitro cells.
Abbreviation: ND, not determined.

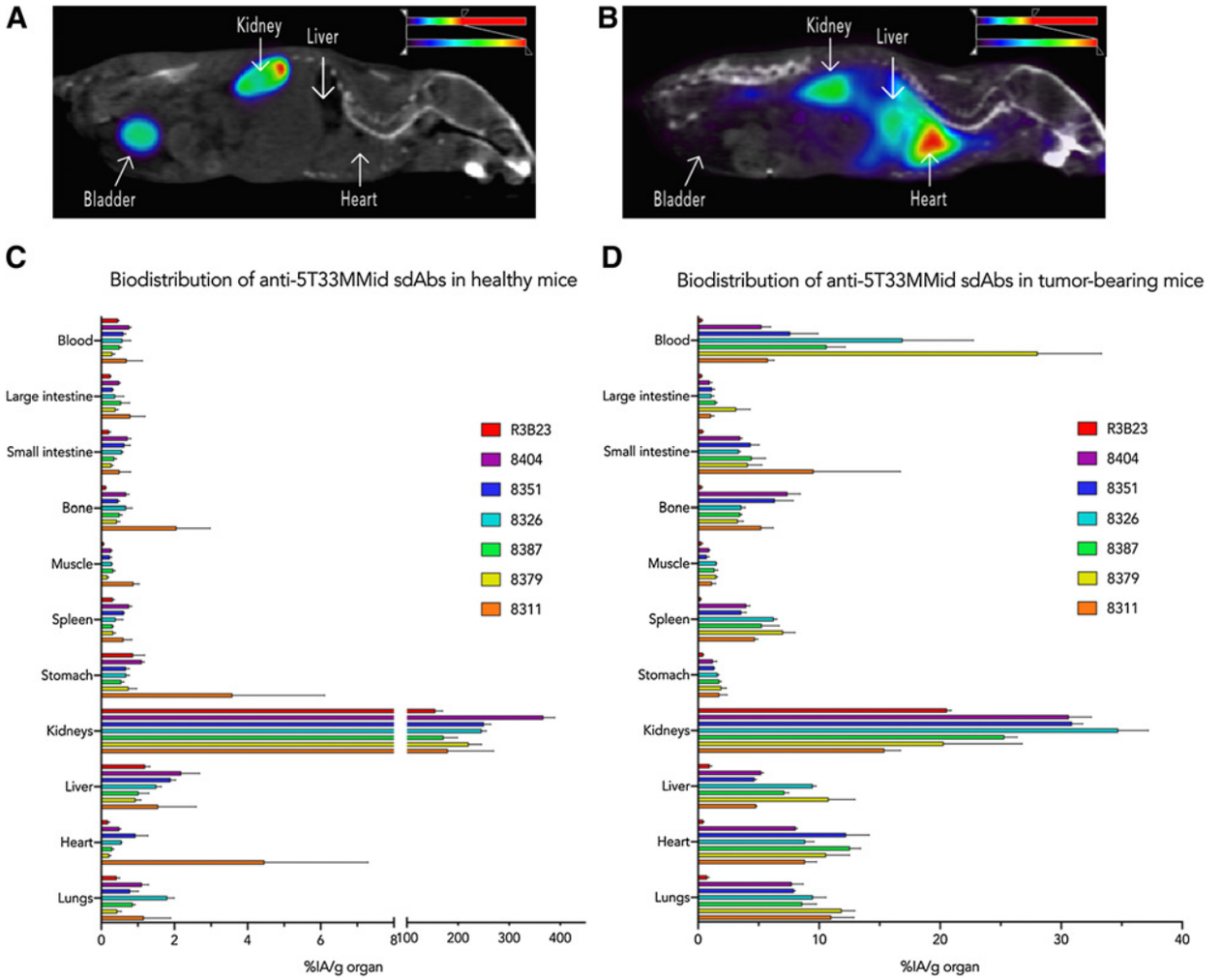

Figure 2.

Biodistribution of ^{99m}Tc-labeled sdAbs in healthy and 5T33MM-bearing mice. Representative sagittal μSPECT/CT images ([^{99m}Tc]-8379) 1 hour after administration of ^{99m}Tc-labeled sdAb in healthy (**A**) and 5T33MM-bearing (**B**) mice. Anti-5T33MM sdAbs show low activity levels in organs of healthy mice, apart from kidneys and bladder. On the contrary, in 5T33MM-bearing mice, sdAbs show high blood pool activity due to binding circulating paraprotein. *Ex vivo* biodistribution analysis of 6 targeting [^{99m}Tc]-sdAb candidates and control [^{99m}Tc]-R3B23 was performed after imaging in healthy (**C**) and 5T33MM-bearing (**D**) mice. Data are based on dissection values (n = 3/sdAb) and displayed as mean ± SD percentage injected activity per gram organ or tissue (%IA/g).

0.5 ± 0.2. Kidney values for diseased mice are significantly lower than their healthy counterparts. Retention of radioactivity in the kidneys of tumor-bearing mice was on average ±11 times lower for all groups, including [^{99m}Tc]-R3B23, signifying renal impairment in the end-organ-damage phase of disease development.

Anti-idiotypic TRNT during the MTD stage reduces tumor burden

Uptake of ^{177}Lu- or ^{225}Ac-labeled sdAb 8379 in different tissues was followed up in time after intravenous administration to determine the absorbed dose in each tissue. Radiochemical purity was above 95% for all radioactive compounds as determined by iTLC (Supplementary Materials and Methods). Organ-absorbed doses for 1 MBq [^{177}Lu]-8379 and 1 kBq [^{225}Ac]-8379 are summarized respectively in Supplementary Tables S2 and S3. Kidneys received the highest absorbed dose of approximately 1 Gy/MBq ^{177}Lu and 0.811 Gy/kBq ^{225}Ac, while all other tissues received a negligible dose from both radionuclides.

The therapeutic efficacy of [^{177}Lu]-8379 and [^{225}Ac]-8379 was investigated in a preclinical murine model resembling MRD. C57BL/KaLwRij mice were intravenously injected with 5T33MMvivo cells and after 4 days—when tumor load is reported to be below 10% and circulating paraprotein levels are undetectable (19)—all animals were treated with either saline buffer, anti-5T2MMid sdAb R3B23 labeled with ^{177}Lu or ^{225}Ac, or anti-5T33MMid sdAb 8379 labeled with ^{177}Lu or ^{225}Ac. Mice treated with [^{177}Lu]-R3B23 showed no significant difference in median survival compared with the saline-treated group (21 vs. 18 days postinjection, respectively), whereas the [^{177}Lu]-8379–treated group showed a 14-day delay in median survival (32 vs. 18 days postinjection, $P < 0.001$; **Fig. 3A**). When seven mice of the saline-treated group reached humane endpoint criteria for euthanasia (day 18 postinoculation for the ^{177}Lu experiment, day 20 postinjection for the

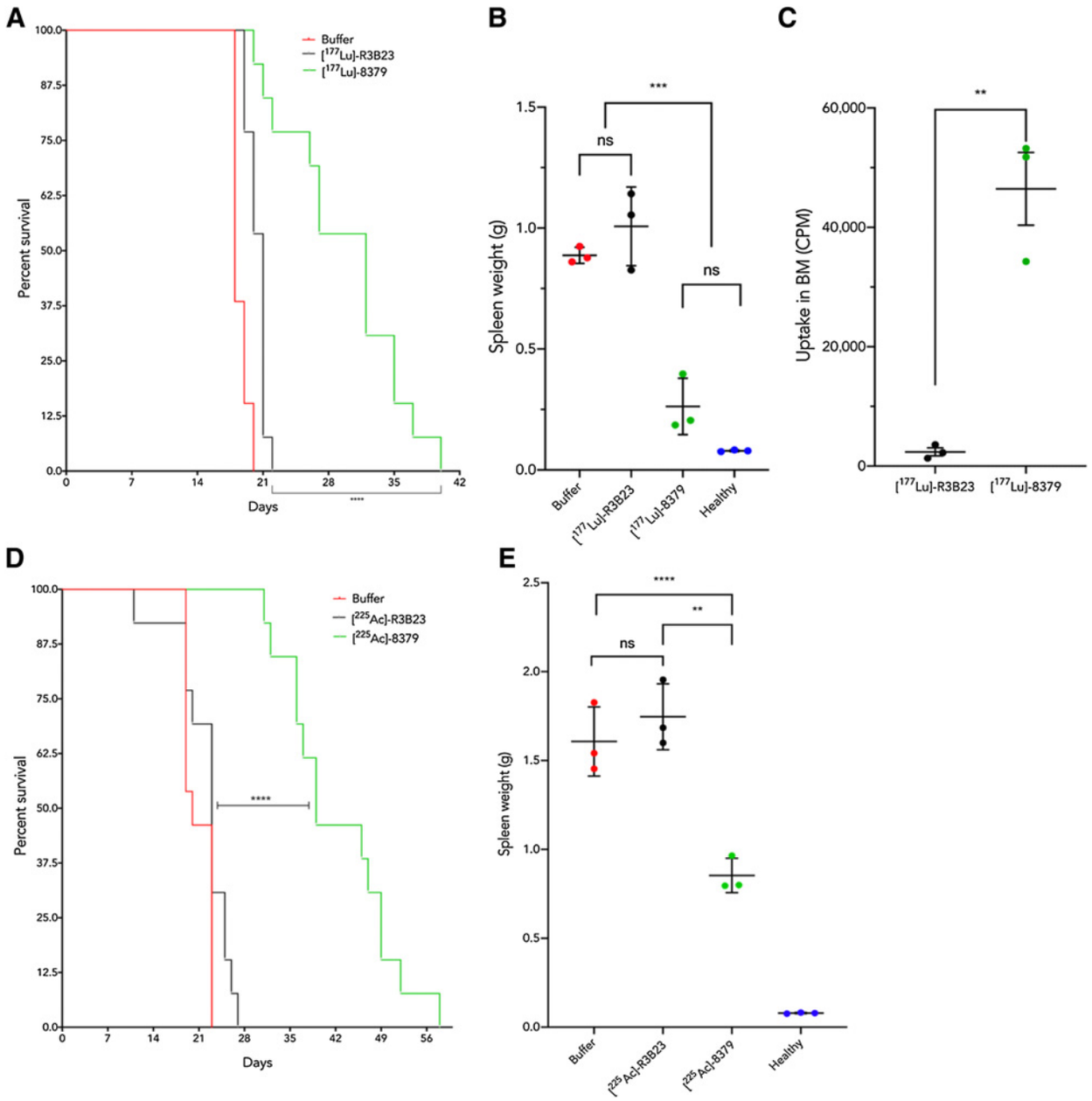

Figure 3.

Therapeutic outcome of anti-idiotype sdAb-based TRNT. **A,** Event-free survival during TRNT with [^{177}Lu]-8379. 5T33MMvivo tumor-bearing mice ($n = 13$/group) were treated with [^{177}Lu]-8379. Control groups received either saline buffer or [^{177}Lu]-R3B23 in equimolar quantities and same activity as treated groups. Treatments were administered on days 4, 7, 10, and 13 after tumor inoculation. **B,** Weight of spleens ($n = 3$/group) were compared at day 18 to assess the degree of splenomegaly. **C,** Tracer uptake in the bone marrow (day 18, $n = 3$/group) was confirmed in [^{177}Lu]-8379–treated mice, whereas there was no uptake of [^{177}Lu]-R3B23. **D,** Event-free survival during TRNT with [^{225}Ac]-8379. 5T33MMvivo tumor-bearing mice ($n = 13$/group) were treated with [^{225}Ac]-8379. Control groups received either saline buffer or [^{225}Ac]-R3B23 in equimolar quantities and same activity as treated groups. Treatments were administered on days 4, 7, 10, and 13 after tumor inoculation. **E,** Weight of spleens ($n = 3$/group) were compared at day 20 to assess the degree of splenomegaly. (ns, not significant; **, $P < 0.01$; ***, $P < 0.001$; and ****, $P < 0.0001$).

^{225}Ac experiment), three animals per group were killed, and tracer uptake in BM was determined via gamma emission detection. The weight of the spleen was measured to assess the degree of splenomegaly. Spleen weights were comparable between saline-treated and R3B23-treated mice ($P > 0.05$). Mice receiving [^{177}Lu]-8379 treatment showed no significantly increased spleen weight compared with healthy non-tumor-bearing, nontreated mice ($P > 0.05$; **Fig. 3B**). The [^{177}Lu]-8379–treated group also showed remarkably higher uptake values in the BM compared with [^{177}Lu]-R3B23–treated mice (47,038 $\pm$ 7,584 CPM vs. 2,386 $\pm$ 1,145 CPM, $P < 0.01$), demonstrating the

in vivo targeting potential of sdAb 8379 for malignant cells within the BM (**Fig. 3C**). Mice treated with [^{225}Ac]-R3B23 revealed no significant difference in median survival compared with the saline-treated group (23 vs. 20 days postinoculation, respectively), whereas the [^{225}Ac]-8379–treated group exhibited a 19-day delay in median survival (39 vs. 20 days postinjection, $P < 0.001$; **Fig. 3D**). [^{225}Ac]-8379–treated mice show significantly lower spleen weights compared with [^{225}Ac]-R3B23–treated mice ($P < 0.01$; **Fig. 3E**). [^{225}Ac]-8379 uptake in the BM was not distinguishable from the background due to the low injected activity. Treatment-related toxicity was most noticeable in the kidneys, with an increased prevalence of slight tubular dilation and basophilia. Notably, [^{225}Ac]-8379–treated and [^{177}Lu]-8379–treated mice showed lower plasma cell infiltration and focal myelofibrosis compared with nontreated or control-treated mice (Supplementary Table S4).

Immunization of a llama with patient-derived serum Ig resulted in highly idiotype-specific sdAbs

Patients with more than 5% of plasma cells in their BM aspirates were included in the clinical study. BM samples were stained for CD38, IgG, IgD, IgA, IgM, and kappa and lambda light chain presence. Malignant plasma cells were selected on the basis of high CD38 expression (Supplementary Fig. S2A). Of 10 patients with sufficient plasma cells, eight were confirmed to have multiple myeloma, one was confirmed with monoclonal gammopathy of unknown significance, and one with solitary plasmacytoma. In seven of eight patients with multiple myeloma, CD38 signals allowed assessment of membrane-anchored paraprotein on malignant plasma cells. In two of seven patients, membrane-expressed paraprotein was considered low or absent. A total of five of seven patients displayed membrane expression of surface Ig.

Of three patients with confirmed surface Ig expression, and with the highest circulating paraprotein titer, serum was taken and purified using protein G affinity chromatography. The protein G–purified antigen (i.e., idiotype-protein G) was used for the immunization of individual llamas and subsequent panning and screening for anti-Id sdAbs. One patient was characterized by the clonal expansion of an isotype IgG-producing plasma cell (patient 2, idiotype P02$_G$id), whereas the other patients displayed the overproduction of isotype IgA paraproteins, one monomeric (patient 5, idiotype P05$_{A,m}$id; Supplementary Fig. S2B–S2D) and one dimeric (patient 1, idiotype P01$_{A,d}$id) IgA.

The sdAb immune library underwent a three-round competitive phage-display panning, and clones were randomly selected from the second and third panning rounds for further screening.

Of 285 tested P05$_{A,d}$id colonies, 141 colonies scored positive in this assay. On the basis of sequence data of the positive colonies, 20 different full-length sdAbs were distinguished, belonging to four different CDR3 groups. Of these 20 sdAbs, only one cross-reacted slightly with human IgM and IgA.

Of 190 tested P01$_{A,m}$id colonies, 181 colonies scored positive in this assay. On the basis of sequence data of the positive colonies, 14 different full-length sdAbs were distinguished, belonging to nine different CDR3 groups (**Fig. 4**).

Of 285 tested P02$_G$id colonies, no colonies scored positive in this assay. None of the obtained sdAbs was able to distinguish between the P02$_G$id IgG and total human IgG.

Discussion

In recent years, the therapeutic approach for multiple myeloma has changed drastically with the growing knowledge of the involvement of the tumor microenvironment in the BM. Yet, the 5-year survival rate remains low at approximately 54%, and most patients will inevitably relapse, with or without acquired multiple drug resistance (20, 21). Despite promising clinical response in the initial treatment stages, patients who achieve complete remission may still experience MRD which often results in disease relapse (22). MRD negativity is therefore

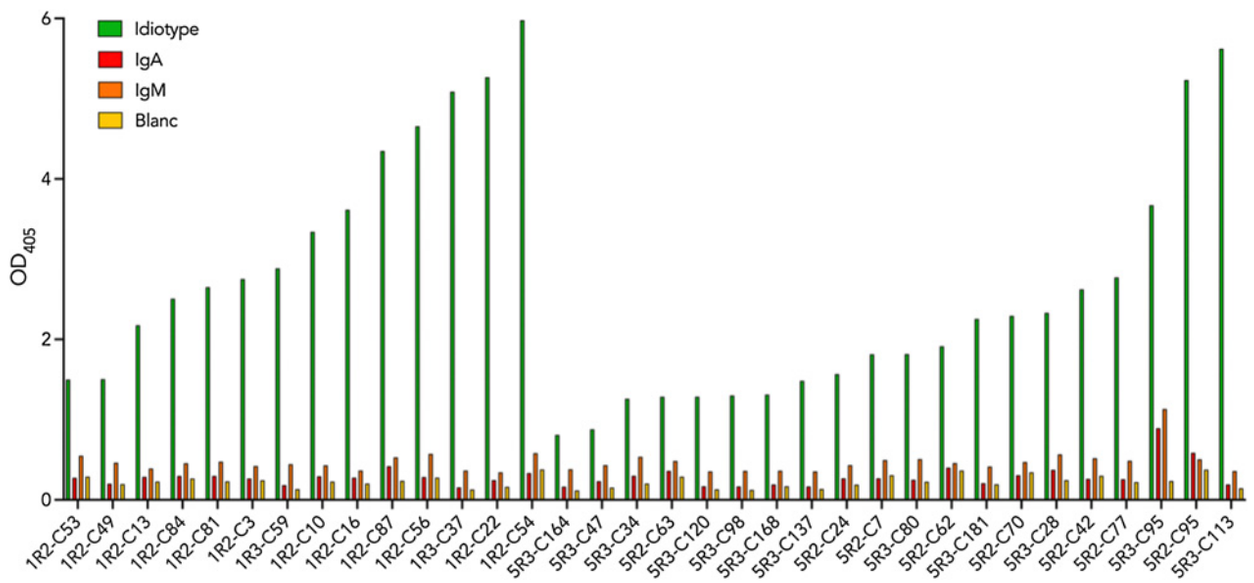

Figure 4.
ELISA readout of anti-idiotypic sdAbs from panning rounds two and three (R2-R3) on immobilized P01$_{A,m}$id-protein G or P05$_{A,d}$id-protein G (green), total human IgA (red), total human IgM (orange), or uncoated wells (yellow). SdAbs were considered as idiotype-specific when the OD$_{405}$(idiotype) ≥ 3× OD$_{405}$(IgA, IgM or blanc).

considered as one of the most significant prognostic factors for long-term survival in multiple myeloma and is likely to become the major focus of treatment development strategies in the future (23, 24). Characterization of relevant biomarkers on dormant cells in the MRD stage is therefore crucial for therapeutic success. Some of the challenges remain the complex heterogeneity of multiple myeloma and expression of traditional multiple myeloma biomarkers on other healthy cell populations (25). It is becoming more apparent that a personalized treatment will provide the most efficient and safest approach for each specific patient (26). In the scarce studies that investigate membrane idiotype expression, it has been reported that in about 35% of diagnosed multiple myeloma cases, the paraprotein is found to be anchored to the surface of malignant plasma cells (6–8). In addition, there is a direct relation between bortezomib resistance and plasma cell maturation stage, whereby bortezomib-resistant malignant cells are distinguished by a decreased Ig secretion and an increased expression of idiotypic paraprotein on their cell surface (27).

In our own cohort study, we have observed idiotypic membrane expression for five of seven patients with multiple myeloma, of which IgG and IgA were the only isotypes present. These results underline the importance and applicability of an idiotype-targeted approach. Because the paraprotein is only expressed on multiple myeloma cells with a high incidence, it offers a cancer-specific target that is ideal to optimize delivery of cytotoxic compounds to the cancer cells while limiting systemic toxicity. Anti-Id vaccination of patients with follicular lymphoma in the MRD stage has shown to elicit a strong antitumor effect and improve clinical outcome. Id-based vaccination has already been evaluated in patients with multiple myeloma using Id-pulsed dendritic cells, yet with varying results (28–32). Autologous Id proved to be only mildly immunogenic, or due to the immunosuppressive multiple myeloma microenvironment only weak to intermediate affinity T cells were generated, which hampers further evaluation of Id-based vaccination strategies in multiple myeloma (33, 34). A way to circumvent these issues is to target Id-expressing multiple myeloma cells with a potent cytotoxic vehicle, bypassing the need to efficiently stimulate the patient's immune system.

In this study, we describe the use of sdAbs for preclinical TRNT in an MRD-like stage of multiple myeloma and assess the feasibility of a sdAb-based personalized myeloma medicine platform for a clinical setting. sdAbs are the smallest antigen-binding fragments derived from camelid heavy-chain-only antibodies and can be generated in a cost-efficient way against a wide variety of proteins (35). Lemaire and colleagues provided the first proof of concept of anti-Id sdAbs, using the murine 5T2MMid model (15). The R3B23 sdAb proved to be an efficient tracer to monitor disease progression *in vivo* and target multiple myeloma cells in an MRD-like setup. It was shown that μSPECT/CT scanning with radiolabeled sdAbs was more sensitive for early detection of M-protein than capillary electrophoresis. These results demonstrated that anti-Id sdAbs are promising vehicles for nuclear diagnostics and TRNT in the MRD stage. However, for the generation of anti-5T2MMid sdAb R3B23 a dromedary was immunized with highly pure 5T2MMid paraprotein of a standard that is not achievable for clinical patient samples.

Here, we take advantage of the abundance of circulating paraprotein present in the murine 5T33MM model to prove the feasibility of patient-specific sdAb generation. Llamas were immunized with the purified IgG fraction from serum taken from either 5T33MMid-bearing mice or patients with circulating paraprotein.

In the first preclinical stage, we evaluated the efficiency of sdAb generation and selection using patient-grade 5T33MMid-containing IgG samples and compared them with the previously used method using highly purified antigen, namely the 5T33MMid. During the initial screening, four out of 10 sdAbs were retrieved using both the 5T33-protein G and 5T33-pure panning, demonstrating that highly specific anti-Id sdAbs can be generated and retrieved using crudely purified IgG fractions from serum.

After extensive screening of sdAb candidates, sdAb 8379 was selected as the lead anti-5T33MMid compound for further evaluation of anti-Id TRNT. Dosimetry analysis in healthy mice showed very low absorbed doses in all organs, apart from kidneys where the administration of a single dose of [^{177}Lu]-8379 resulted in 1.019 Gy/MBq and [^{225}Ac]-8379 resulted in 0.811 Gy/kBq due to slow renal clearance of the radiotracer, despite the co-administration of Gelofusine (Supplementary Tables S1 and S2). This makes the kidneys one of the dose-limiting organs for TRNT, as is the case for almost all radiotracers that are smaller than the size cutoff for renal clearance. However, because this sdAb has a remarkably higher renal retention compared with previous clinically validated sdAbs, therapeutic doses were calculated to remain under 2 Gy delivered to the BM. However, due to the absence of malignant plasma cells, the determined dose to the BM might be underestimated. The total cumulative dose to the BM was therefore limited to 1.5 Gy during the treatment regimen.

Early-stage 5T33MMid-diseased mice—resembling residual cells nested in the BM—experienced significant survival benefit from [^{177}Lu]-8379 treatment compared with untreated mice (32 days vs. 18 days, 77.8% increase in median survival, $P < 0.0001$) or mice treated with the ^{177}Lu-labeled anti-5T2MMid sdAb R3B23 (32 vs. 21 days, $P < 0.0001$). This demonstrates the ability of anti-Id sdAbs to discriminate between two different idiotypes.

Because the spleen is a hematopoietic organ in mice, it harbors malignant plasma cells during disease progression. Splenomegaly is therefore a common feature in the syngeneic 5T33MM myeloma model. The [^{177}Lu]-8379–treated group showed no significant difference in spleen weight compared with naïve, nontreated mice. Control groups show a significantly higher spleen weight than treated groups. Tracer uptake in the BM was confirmed in [^{177}Lu]-8379–treated mice, whereas there was no uptake of [^{177}Lu]-R3B23. The efficacy of anti-idiotypic β^--TRNT has been shown now in the 5T33MMid model and previously with the 5T2MMid model. To increase the therapeutic potential of anti-Id sdAbs, the use of α-particle emitting radionuclides might further improve their targeted cytotoxicity toward multiple myeloma cancer cells. α-particles are characterized by a high energy deposition of a short distance of merely a few cell diameters. This results in a higher linear energy transfer compared with β^--particles.

To that end, sdAb-based targeted α-therapy has been evaluated in 5T33MMid-disease bearing mice. Mice receiving [^{225}Ac]-8379 treatment experienced a significant prolonged survival compared with control-treated animals (39 vs. 20 days, 95.0% increase in median survival, $P < 0.0001$) and a significant delay in end-organ damage. Radioactive compound uptake in the BM was indistinguishable from the background signal due to the low injected activity of the ^{225}Ac-labeled sdAbs, signifying the potency of α-particles compared with β^--particles.

Radiolabeled anti-idiotypic sdAbs exert strong antitumor activity during MRD-like disease in this preclinical model for multiple myeloma. Because of the high selectivity of anti-Id radioimmunoconjugates, off-target toxicity in healthy tissues is minimized, as is confirmed by the biodistribution profile and toxicity analysis (Supplementary Table S4). Not only does this allow optimization of the therapeutic window, but the low background interference could provide sensitive detection of circulating paraprotein or lesions caused by residual cancer cells at the moment of disease recurrence. This emphasizes

the diagnostic, predictive, and therapeutic value of the anti-Id sdAb platform. In addition, the economically favorable and fast generation of sdAb libraries adds merit to the feasibility of large-scale personalized multiple myeloma treatment (36). Time for sdAb generation could be further reduced by performing a preemptive screening of available synthetic sdAb libraries which would circumvent the need for immunization (37). Non–animal-derived sdAb selection might also aid in reducing the significant cost of GMP production of patient-tailored sdAbs.

Successful camelid immunization using murine protein G–purified serum containing an abundance of paraprotein and the retrieval of a plethora of idiotype-selective sdAbs therefore demonstrated the feasibility of patient-specific sdAb generation and their promising value for personalized TRNT. Immunization of a llama with purified sera obtained from patients with multiple myeloma with confirmed membrane-expressed paraprotein on malignant plasma cells in the BM led to the generation of highly patient-specific sdAbs for two of three patients. For two patients who were diagnosed with either a monomeric or dimeric IgA isotype paraprotein, the murine-tested sdAb generation procedure resulted in 14 and 20 different sdAb candidates, respectively. These findings confirm the possibility of applying the sdAb generation platform for highly personalized targeted therapy of patients with multiple myeloma with membrane expression of their respective paraproteins. Not only do these results confirm the claim that malignant plasma cells do regularly present membrane-bound paraprotein, but that these paraproteins can serve as therapeutic target in the absence of circulating paraprotein during MRD or when other multiple myeloma–relevant target proteins are absent (5).

Remarkably, none of the obtained sdAbs was able to distinguish between the $P02_{G}$id IgG and total human IgG. The inability of generating anti-Id sdAbs toward IgG-structured paraprotein might originate in the limited purity of the antigen mixture used for immunization and screening, a dominant immune response toward common epitopes on IgG antibodies, or a lack of immunogenicity of the patient's CDR domain. Whether this occurrence is an anomaly or embodies a recurring problem for IgG-isotype paraproteins remains to be seen in further investigation. Considering that IgG is the most prevalent isotype in serum (38), it is likely that any contaminants after protein G purification will be of the IgG isotype, thus hindering a paraprotein-specific immunization and selection. Nonetheless, the efficiency at which sdAbs could be generated targeting murine IgG-structured paraproteins shows that theoretically, sdAbs can be generated against a myriad of paraproteins.

The production of patient-tailored anti-Id sdAbs can be initiated during first-line standard of care, and be applied as TRNT agents after achieving complete remission to obtain the MRD-negative state. The ease of paraprotein isolation from patients and subsequent immunization of camelids, combined with the fast, cost-efficient sdAb generation and selection, offers a platform for truly personalized medicine for patients with multiple myeloma with a high degree of relapse. Radiolabeled sdAbs are promising therapeutic vehicles to avoid disease relapse or even achieve the much-desired state of MRD negativity.

Authors' Disclosures

J. Puttemans reports personal fees from Fonds Wetenschappelijk Onderzoek (FWO) and grants from Stichting Tegen Kanker and Fonds Wetenschappelijk Onderzoek (FWO-V, grant I001618N) during the conduct of the study. M. Keyaerts reports non-financial support from Abscint during the conduct of the study; grants from Precirix outside the submitted work; in addition, M. Keyaerts has patents on the use of nanobodies for imaging and therapy issued, and licensed to Abscint. H. Hanssens reports personal fees from Fonds Wetenschappelijk Onderzoek Vlaanderen (FWO) during the conduct of the study. T. Lahoutte reports personal fees from Precirix and Abscint during the conduct of the study; in addition, T. Lahoutte has a patent US20160030606 issued to VUB and a patent WO2017013026A1 issued to VUB. N. Devoogdt reports grants from Stichting Tegen Kanker and Research Foundation-Flanders (FWO) during the conduct of the study; grants, personal fees, nonfinancial support, and other support from Precirix; non-financial support and other support from Abscint, grants from Esobiotech; grants from Exevir, Confo Therapeutics, Roche, and Telix Pharma outside the submitted work. M. D'Huyvetter reports grants from Stichting tegen kanker and Fonds Wetenschappelijk Onderzoek (FWO) during the conduct of the study; personal fees from Precirix SA outside the submitted work; in addition, M. D'Huyvetter has a patent for the use of sdAbs for diagnosis and therapy issued and a patent for use of sdAbs for diagnosis and therapy pending. No disclosures were reported by the other authors.

Authors' Contributions

J. Puttemans: Conceptualization, formal analysis, investigation, visualization, methodology, writing–original draft, project administration. **B. Stijlemans:** Conceptualization, software, formal analysis, investigation. **M. Keyaerts:** Conceptualization, methodology. **S. Vander Meeren:** Investigation, methodology. **W. Renmans:** Formal analysis, investigation. **K. Fostier:** Conceptualization. **P. Debie:** Investigation. **H. Hanssens:** Investigation. **M. Rodak:** Investigation. **M. Pruszynski:** Resources, supervision. **K. De Veirman:** Investigation. **K. Vanderkerken:** Resources, writing–review and editing. **T. Lahoutte:** Resources. **A. Morgenstern:** Resources. **F. Bruchertseifer:** Resources. **N. Devoogdt:** Conceptualization, supervision, funding acquisition, methodology, writing–review and editing. **M. D'Huyvetter:** Conceptualization, resources, supervision, funding acquisition, methodology, project administration, writing–review and editing.

Acknowledgments

The authors would like to thank Jurgen Haustraete (Protein Service facility, VIB, Ghent, Belgium), Gholamreza Hassanzadeh Ghassabeh and Steve Schoonooghe (Nanobody Service Facility, VIB, Brussels, Belgium), Jan De Jonge and Pinky Sharma for their technical assistance. The authors would like to thank Yasmine De Maeyer (UZ Brussel, Brussels, Belgium) for her assistance in managing patient data.

This study was supported by grant funding from the Stichting Tegen Kanker (Translational & Clinical Research Grant 1635, 2016), and travel, infrastructure and research funding from Research Foundation-Flanders (FWO; G028220N, I001618N and VS02919N). J. Puttemans and H. Hanssens received a personal predoctoral mandate from FWO. M. D'Huyvetter. and K. De Veirman are postdoctoral fellows of FWO, and T. Lahoutte and M. Keyaerts are senior clinical investigators of FWO. M. Rodak was funded by Operational Project Knowledge Education Development, co-financed by the European Social Fund (POWR.03.02.00-00-I009/17-00).

The costs of publication of this article were defrayed in part by the payment of page charges. This article must therefore be hereby marked *advertisement* in accordance with 18 U.S.C. Section 1734 solely to indicate this fact.

Received March 9, 2021; revised May 25, 2021; accepted October 11, 2021; published first October 19, 2021.

References

1. Pawlyn C, Jackson GH. Physicians, paraproteins and progress: diagnosis and management of myeloma. Br J Hosp Med 2019;80:91–8.
2. Kumar SK, Dispenzieri A, Lacy MQ, Gertz MA, Buadi FK, Pandey S, et al. Continued improvement in survival in multiple myeloma: changes in early mortality and outcomes in older patients. Leukemia 2014;28:1122–8.
3. Kristinsson SY, Landgren O, Dickman PW, Derolf AR, Björkholm M. Patterns of survival in multiple myeloma: a population-based study of patients diagnosed in Sweden from 1973 to 2003. J Clin Oncol 2007;25:1993–9.
4. Koreth J, Cutler CS, Djulbegovic B, Behl R, Schlossman RL, Munshi NC, et al. High-dose therapy with single autologous transplantation versus chemotherapy

for newly diagnosed multiple myeloma: a systematic review and meta-analysis of randomized controlled trials. Biol Blood Marrow Transplant 2007;13:183–96.
5. Matsui W, Wang Q, Barber JP, Brennan S, Smith BD, Borrello I, et al. Clonogenic multiple myeloma progenitors, stem cell properties, and drug resistance. Cancer Res 2008;68:190–7.
6. Ghosh N, Matsui W. Cancer stem cells in multiple myeloma. Cancer Lett 2009; 277:1–7.
7. Ocqueteau M, San Miguel JF, González M, Almeida J, Orfao A. Do myelomatous plasma cells really express surface immunoglobulins? Haematologica 1996;81: 460–3.
8. Wen YJ, Barlogie B, Yi Q. Idiotype-specific cytotoxic T lymphocytes in multiple myeloma: evidence for their capacity to lyse autologous primary tumor cells. Blood 2001;97:1750–5.
9. Khoo WH, Ledergor G, Weiner A, Roden DL, Terry RL, McDonald MM, et al. A niche-dependent myeloid transcriptome signature defines dormant myeloma cells. Blood 2019;134:30–43.
10. Debie P, Lafont C, Defrise M, Hansen I, van Willigen DM, van Leeuwen FWB, et al. Size and affinity kinetics of nanobodies influence targeting and penetration of solid tumours. J Control Release 2020;317:34–42.
11. Hassanzadeh-Ghassabeh G, Devoogdt N, De Pauw P, Vincke C, Muyldermans S. Nanobodies and their potential applications. Nanomedicine 2013;8:1013–26.
12. Muyldermans S. Nanobodies: natural single-domain antibodies. Annu Rev Biochem 2013;82:775–97.
13. Vanderkerken K, De Raeve H, Goes E, Van Meirvenne S, Radl J, Van Riet I, et al. Organ involvement and phenotypic adhesion profile of 5T2 and 5T33 myeloma cells in the C57BL/KaLwRij mouse. Br J Cancer 1997;76:451–60.
14. Asosingh K, Radl J, Van Riet I, Van Camp B, Vanderkerken K. The 5TMM series: a useful *in vivo* mouse model of human multiple myeloma. Hematol J 2000;1: 351–6.
15. Lemaire M, D'Huyvetter M, Lahoutte T, Van Valckenborgh E, Menu E, De Bruyne E, et al. Imaging and radioimmunotherapy of multiple myeloma with anti-idiotypic Nanobodies. Leukemia 2014;28:444–7.
16. Vincke C, Gutierrez C, Wernery U, Devoogdt N, Hassanzadeh-Ghassabeh G, Muyldermans S. Generation of single domain antibody fragments derived from camelids and generation of manifold constructs. Methods Mol Biol 2012;907: 145–76.
17. Loening AM, Gambhir SS. AMIDE: a free software tool for multimodality medical image analysis. Mol Imaging 2003;2:131–7.
18. D'Huyvetter M, Vincke C, Xavier C, Aerts A, Impens N, Baatout S, et al. Targeted radionuclide therapy with A 177Lu-labeled anti-HER2 nanobody. Theranostics 2014;4:708–20.
19. De Veirman K, Van Ginderachter JA, Lub S, De Beule N, Thielemans K, Bautmans I, et al. Multiple myeloma induces Mcl-1 expression and survival of myeloid-derived suppressor cells. Oncotarget 2015;6:10532–47.
20. Ghobrial I. Multiple myeloma: statistics. In Multiple Myeloma Guide; 2020. American Society of Clinical Oncology. Available from: https://www.cancer.net/cancer-types/multiple-myeloma/statistics.
21. Robak P, Drozdz I, Szemraj J, Robak T. Drug resistance in multiple myeloma. Cancer Treat Rev 2018;70:199–208.
22. Luskin MR, Murakami MA, Manalis SR, Weinstock DM. Targeting minimal residual disease: a path to cure? Nat Rev Cancer 2018;18:255–63.
23. Romano A, Palumbo GA, Parrinello NL, Conticello C, Martello M, Terragna C. Minimal residual disease assessment within the bone marrow of multiple myeloma: a review of caveats, clinical significance and future perspectives. Front Oncol 2019;9:699.
24. Landgren O, Iskander K. Modern multiple myeloma therapy: deep, sustained treatment response and good clinical outcomes. J Intern Med 2017;281:365–82.
25. Levin A, Hari P, Dhakal B. Novel biomarkers in multiple myeloma. Transl Res 2018;201:49–59.
26. Pawlyn C, Davies FE. Toward personalized treatment in multiple myeloma based on molecular characteristics. Blood 2019;133:660–75.
27. Leung-Hagesteijn C, Erdmann N, Cheung G, Keats JJ, Stewart AK, Reece DE, et al. Xbp1s-negative tumor B cells and pre-plasmablasts mediate therapeutic proteasome inhibitor resistance in multiple myeloma. Cancer Cell 2013;24: 289–304.
28. Yi Q, Szmania S, Freeman J, Qian J, Rosen NA, Viswamitra S, et al. Optimizing dendritic cell-based immunotherapy in multiple myeloma: intranodal injections of idiotype-pulsed CD40 ligand-matured vaccines led to induction of type-1 and cytotoxic T-cell immune responses in patients. Br J Haematol 2010;150:554–64.
29. Curti A, Tosi P, Comoli P, Terragna C, Ferri E, Cellini C, et al. Phase I/II clinical trial of sequential subcutaneous and intravenous delivery of dendritic cell vaccination for refractory multiple myeloma using patient-specific tumour idiotype protein or idiotype (VDJ)-derived class I-restricted peptides. Br J Haematol 2007;139:415–24.
30. Reichardt VL, Milazzo C, Brugger W, Einsele H, Kanz L, Brossart P. Idiotype vaccination of multiple myeloma patients using monocyte-derived dendritic cells. Haematologica 2003;88:1139–49.
31. Hansson L, Abdalla AO, Moshfegh A, Choudhury A, Rabbani H, Nilsson B, et al. Long-term idiotype vaccination combined with interleukin-12 (IL-12), or IL-12 and granulocyte macrophage colony-stimulating factor, in early-stage multiple myeloma patients. Clin Cancer Res 2007;13:1503–10.
32. Massaia M, Borrione P, Battaglio S, Mariani S, Beggiato E, Napoli P, et al. Idiotype vaccination in human myeloma: generation of tumor-specific immune responses after high-dose chemotherapy. Blood 1999;94:673–83.
33. Ruffini PA, Neelapu SS, Kwak LW, Biragyn A. Idiotypic vaccination for B-cell malignancies as a model for therapeutic cancer vaccines: from prototype protein to second generation vaccines. Haematologica 2002;87:989–1001.
34. Rhee F. Idiotype vaccination strategies in myeloma: how to overcome a dysfunctional immune system. Clin Cancer Res 2007;13:1353–5.
35. Hamers-Casterman C, Atarhouch T, Muyldermans S, Robinson G, Hamers C, Songa EB, et al. Naturally occurring antibodies devoid of light chains. Nature 1993;363:446–8.
36. Chanier T, Chames P. Nanobody engineering: toward next generation immunotherapies and immunoimaging of cancer. Antibodies 2019;8:13.
37. Rothbauer U. Speed up to find the right ones: rapid discovery of functional nanobodies. Nat Struct Mol Biol 2018;25:199–201.
38. Gonzalez-Quintela A, Alende R, Gude F, Campos J, Rey J, Meijide LM, et al. Serum levels of immunoglobulins (IgG, IgA, IgM) in a general adult population and their relationship with alcohol consumption, smoking and common metabolic abnormalities. Clin Exp Immunol 2008; 151:42–50.